RSC Advances

ROYAL SOCIETY OF CHEMISTRY

www.rsc.org/advances

Journal Name

ARTICLE

Push-pull ruthenium diacetylide complexes: new dyes for p-type dye-sensitized solar cells

Received 00th January 20xx,
Accepted 00th January 20xx

DOI: 10.1039/x0xx00000x

www.rsc.org/

Siliu Lyu,[a] Yoann Farré,[b] Laurent Ducasse,[a] Yann Pellegrin,[b] Thierry Toupance,[a] Céline Olivier*[a] and Fabrice Odobel*[b]

A couple of novel donor-π-acceptor dyes based on organometallic ruthenium diacetylide complexes (**SL1** and **SL2**) have been designed and synthesized for use in NiO-based p-type dye-sensitized solar cells (p-DSCs). The optical and electrochemical properties of the dyes were assessed and theoretical calculations were performed to rationalize the experimental data. The best performing dye in NiO-based p-DSC device is the red dye **SL1** which gives a photocurrent density of 2.25 mA.cm^{-2} and maximum IPCE of 18 %. This represents a promising result, paving the way for future finely tuned organometallic efficient dyes for such application.

Introduction

Ruthenium polypyridine complexes are the archetypal dyes for solar energy conversion as they were abundantly used for water splitting,[1-2] and as sensitizers in conventional n-type dye-sensitized solar cells[3-4] (n-DSCs) (also known as Grätzel cells) and more recently in p-type dye-sensitized solar cells (p-DSCs).[5-7] However, ruthenium organometallic dyes are less investigated for the latter purposes. Some of us recently reported that Ru-diacetylide complexes are however valuable visible-light sensitizers and they can exhibit high photoconversion efficiencies (PCEs) in conventional n-type DSCs. [8-9] In p-DSCs a p-type semiconductor (p-SC), usually NiO, is sensitized by a dye according to a reductive quenching mechanism, that is a hole photoinjection into the valence band of the p-SC.[10-11] Several classes of dyes were designed for p-DSCs, including push-pull organic sensitizers,[12-14] perylene imides,[15-17] diketopyrrolopyrroles,[18] squaraines,[19-20] BODIPYs,[21-22] porphyrins,[23-25] ruthenium[5-7,26] and iridium[27] polypyridine complexes. Ruthenium diacetylide complexes are neutral molecules, display easily tunable electronic properties and their rod-like structure enables to prepare push-pull systems. All these properties make them attractive candidates for p-DSCs, because neutral dyes can reach much higher packing density on the SC than charged dyes and a strong push-pull character enhances the charge transfer band which is also favourable for charge injection.[28]

Here we report the first organometallic dyes based on the [Ru(dppe)$_2$] moiety for p-type DSCs. The molecular structure of the new photosensitizers is depicted in Chart 1. The bis(σ-arylacetylide) complexes **SL1** and **SL2** are endowed with a bidentate anchoring group based on a triphenylamine (TPA) as electron-donating unit and are functionalized with an electron-withdrawing group, both separated by a bithiophene linker.

The two new dyes **SL1** and **SL2** were characterized in details showing that ruthenium diacetylide complexes are promising sensitizers for NiO since **SL1** led to significant performances in p-DSCs compared to previously reported dyes for such application.[5-7]

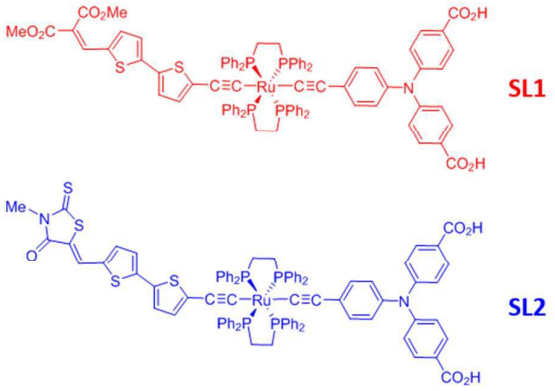

Chart. 1 Molecular structures of the push-pull organometallic dyes **SL1** and **SL2**.

[a] Institut des Sciences Moléculaires, UMR CNRS 5255, Université de Bordeaux, 351 cours de la Libération 33405 Talence Cedex, France. E-mail: c.olivier@ism.u-bordeaux1.fr; Tel: + 33 5 40 00 24 25.
[b] CEISAM, Chimie et Interdisciplinarité, Synthèse, Analyse, Modélisation, UMR CNRS 6230, Faculté des Sciences et des Techniques de Nantes, 2 rue de la Houssinière, Nantes Cedex 3, France. E-mail: Fabrice.Odobel@univ-nantes.fr; Tel: + 33 2 51 12 54 29.

Electronic Supplementary Information (ESI) available: [Schematic view of p-type DSC; Fluorescence emission spectra; Cyclic voltammograms; TD-DFT simulated absorption spectra; NMR and HR-MS data]. See DOI: 10.1039/x0xx00000x

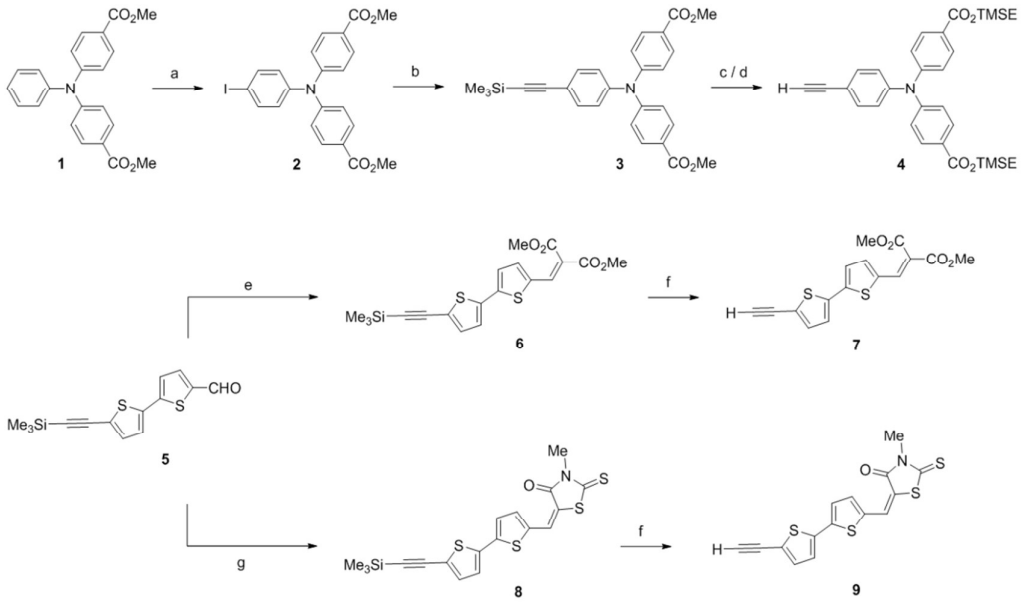

Scheme 1. Synthesis of the alkyne ligands. *Reaction conditions:* (a) ICl, $Zn(OAc)_2$, dioxane; (b) Trimethylsilylacetylene, $PdCl_2(PPh_3)_2$, CuI, DIPEA, THF; (c) LiOH, THF/H_2O; (d) Trimethylsilylethanol, HBTU, DIPEA, DMF; (e) Dimethyl malonate, piperidine, $CHCl_3$; (f) K_2CO_3, MeOH; (g) 3-Methylrodhanine, ammonium acetate, acetic acid.

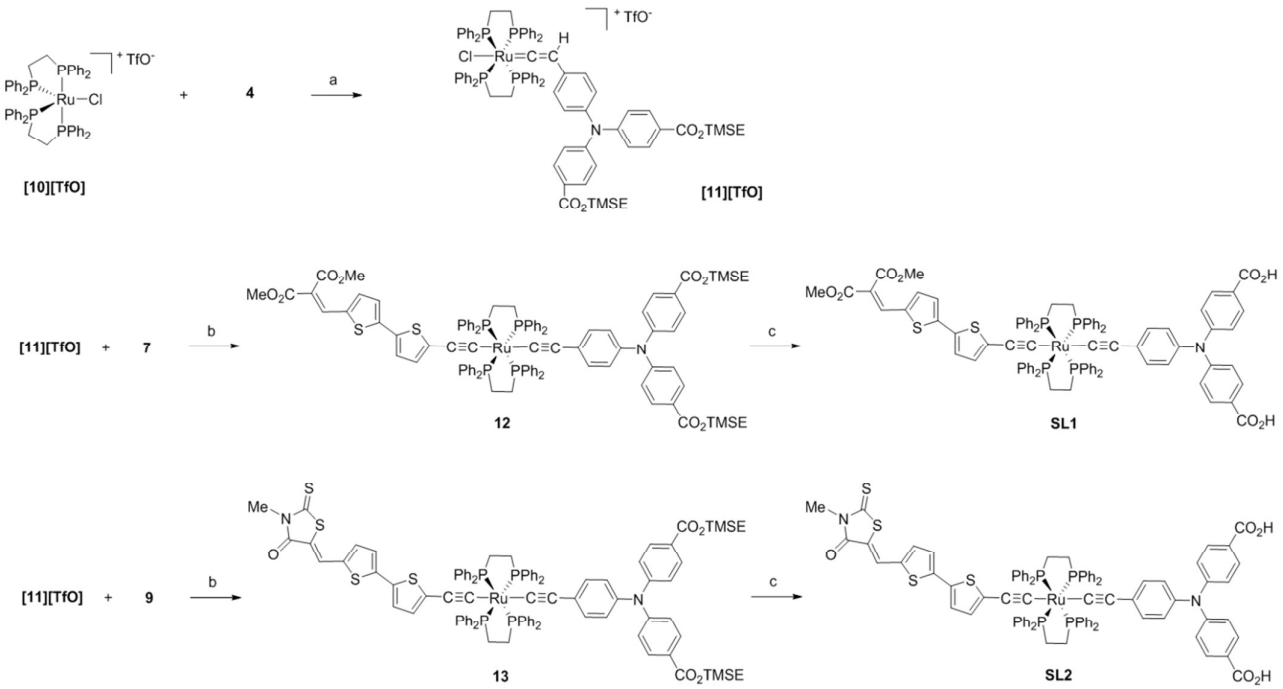

Scheme 2. Synthesis of the organometallic complexes. *Reaction conditions:* (a) CH_2Cl_2; (b) $NaPF_6$, Et_3N, CH_2Cl_2; (c) Tetrabutylammonium fluoride, THF.

Results and discussion

Synthesis of the dyes

Following already established procedures, the preparation of ruthenium-diacetylide complexes consists of successive activation of terminal alkynes by an electron-deficient metal center, typically $[RuCl(dppe)_2][TfO]$.[29] First, the three alkyne ligands **4**, **7** and **9** were prepared following synthetic routes shown on Scheme 1. Synthesis of the TPA-based electron-rich ligand **4** involved Sonogashira coupling reaction of the iodo-TPA

derivative **2** with trimethylsilylacetylene and subsequent deprotection of the terminal alkyne. To avoid side reactions of the carboxylic acid anchoring groups with the metal center during ensuing syntheses, protection of the two COOH functions was necessary. A silyl-ester protecting group, i. e. 2-(trimethylsilyl)ethyl (TMSE), was preferably chosen rather than methyl or *tert*-butyl ester group as the former can be removed under mild conditions. On the other hand, synthesis of the electron-withdrawing σ-alkynyl ligands **7** and **9** was achieved through condensation of the carbaldehyde **5** with dimethyl malonate or 3-methylrodhanine, respectively. The synthetic steps to the target organometallic dyes are represented in Scheme 2. The donor part of the dyes was first obtained by activation of the TPA-based ligand **4** by the 16-electron species **[10][TfO]**, leading to the stable ruthenium-vinylidene intermediate **[11][TfO]**. Subsequent introduction of the second carbon-rich chain on the [Ru(dppe)$_2$] metal centre to form bis-σ-arylacetylide complexes was achieved by reacting **[11][TfO]** with the alkynyl ligands **7** or **9**, in the presence of a base (Et_3N) and of a non-coordinating salt ($NaPF_6$). Finally, the target dyes **SL1** and **SL2** were obtained in good yields after removal of the silyl-ester protecting groups, using tetrabutylammonium fluoride in THF at room temperature.

All the organometallic complexes were characterized by means of ^{31}P, ^{1}H and ^{13}C NMR, HR-MS and FTIR. The full data set is in accordance with the expected structure of the organometallic dyes. The *trans*-ditopic geometry of the ruthenium center in **SL1** and **SL2** was evidenced by ^{31}P NMR as the spectra show a singlet for the four equivalent phosphorus atoms, with $\delta \approx 53$ ppm characteristic of the ruthenium-diacetylide structure.[29] In addition, an intense band was observed on the FT-IR spectra of **SL1** and **SL2** at *ca.* 2038 cm^{-1} corresponding to the $\nu_{C\equiv C}$ stretch of the σ-diacetylide metal fragment.

Optical and electrochemical properties

UV-visible absorption spectra of **SL1** and **SL2**, recorded in dichloromethane solution, are shown in Fig. 1 and the corresponding values are listed in Table 1. The intense short-wavelength absorption band observed in the UV region is characteristic of n → π* and π → π* transitions from the dppe ligands.[30] The less intense band centred around λ = 360 nm can be tentatively ascribed to electronic transitions involving the triphenylamine electron donor, the origin of this band is discussed below. However the most interesting feature of these dyes is the broad absorption band observed in the visible part of the spectrum. This intense absorption band corresponds to multiple metal–ligand charge–transfer (MLCT) processes, mainly stemming from the metal-centred HOMO (highest occupied molecular orbital) to the LUMO (lowest unoccupied molecular orbital) located on the electron–withdrawing alkynyl ligand (see DFT calculations below). The maximum absorption wavelength, λ_{max}, of **SL1** in the visible is centred at 521 nm, making **SL1** a red pigment. Elongation of the π-conjugated system through the rhodanine acceptor group in **SL2** led to red-shifted absorption band. The spectrum of **SL2** shows λ_{max} = 603 nm, hence affording blue-coloured dye-bath solution. Both dyes present a rather high molecular extinction coefficient (ε) of about 20 000 M^{-1} cm^{-1} at λ_{max}. Overall, the good absorption properties of this couple of organometallic complexes make them good candidates for use as photosensitizers in DSCs.

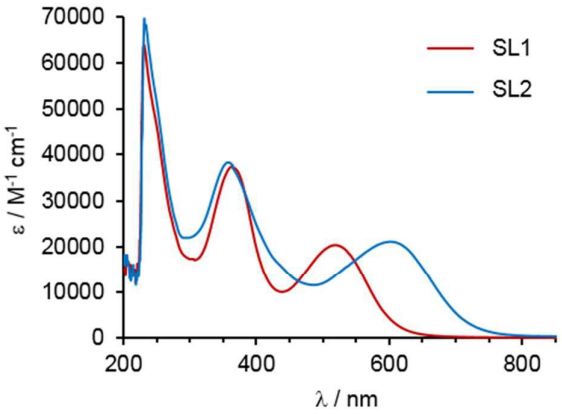

Fig. 1 Absorption spectra of **SL1** and **SL2** in CH_2Cl_2 (C ≈ 3.10^{-5} M).

Although such organometallic complexes are only weakly emissive, fluorescence spectra of **SL1** and **SL2** could be recorded in dichloromethane solution (Fig. S2). The maximum emission wavelength was detected at λ_{em} = 618 nm and λ_{em} = 700 nm for **SL1** and **SL2**, respectively (see ESI). The energy of the excited state (E_{00}) was estimated from the wavelength at the intersection of the normalized absorption and emission spectra. As expected, the blue dye **SL2** presents a lower lying excited state (E_{00} = 1.89 eV) than that of the red dye **SL1** (E_{00}= 2.18 eV).

Table 1. Optical and electrochemical properties.

Dye	λ_{max} [a] (nm)	ε (M^{-1}.cm^{-1})	λ_{em} [b] (nm)	E_{00} [c] (eV)	E_{ox1} [d] (V)	E_{ox2} [d] (V)	E_{red} [d] (V)	E_{red}* [e]
SL1	364	37 500	618	2.18	+0.64	+1.05	–1.39	0.79
	521	20 300						
SL2	359	38 300	700	1.89	+0.54	+0.84	–1.03	0.86
	603	21 050						

[a] Absorption maxima in CH_2Cl_2 solution (C = 3 x 10^{-5} M). [b] Emission maximum in CH_2Cl_2 solution (C = 3 x 10^{-5} M). [c] ΔE_{opt} estimated from the intercept of the normalized absorption and emission spectra. [d] Potentials measured in THF solution with $FeCp_2$ as internal reference and referred to NHE by addition of 630 mV.[31] [e] Reduction potential at the excited state estimated from E_{red}+E_{00}.

The electrochemical properties of **SL1** and **SL2** were investigated by cyclic voltammetry in THF solution (Fig. S3), the corresponding data are gathered in Table 1. In the anodic region, the voltammograms show two reversible monoelectronic processes, both stemming from oxidation of the central electron-rich π-conjugated system with strong contribution of the [Ru(dppe)$_2$] metal fragment. In the cathodic region the voltammograms feature a reversible monoelectronic reduction process mostly centred on the electron withdrawing group (acrylic ester or rodhanine). **SL1** exhibits a more cathodic reduction potential compared to that of **SL2** in agreement with the stronger withdrawing acceptor strength of rodhanine compared to acrylic ester. The calculated reduction potential of the dye at the excited state at + 0.79 V and + 0.86 V *vs.* NHE for **SL1** and **SL2**, respectively, is more positive than the valence band edge of NiO (E_{VB} ~ + 0.54 V *vs.* NHE).[32] This indicates that there is a small but sufficient driving force (about 0.25-0.3 eV) for hole injection from the dye excited state into the valence band of the semiconductor (Table 1). On the other hand, the reduction potential of the dyes is strongly negative, suggesting that regeneration of the dyes by $I_3^-/I_2^{-\bullet}$ (E° = – 0.08 V *vs.* NHE)[33] is a very exergonic process (IΔGI > 0.9 eV) and should operate efficiently within the device.

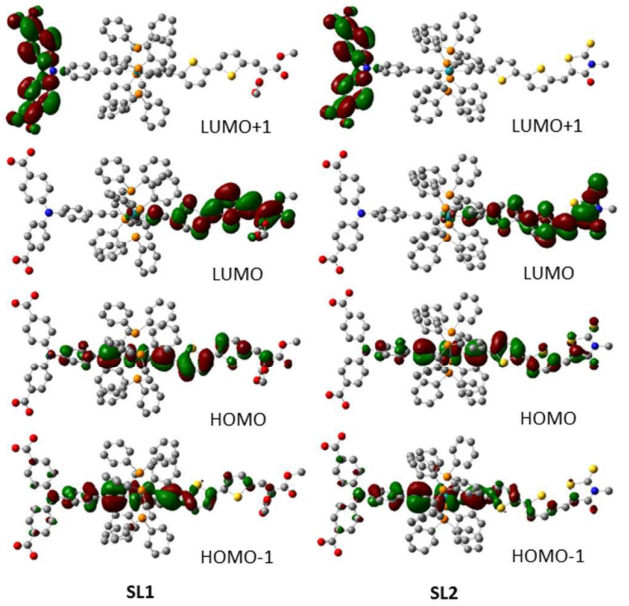

Fig. 2. Electron-density distribution of the transition-involved frontier molecular orbitals of **SL1** and **SL2**.

Theoretical calculations

To gain further insights into the electronic properties of **SL1** and **SL2**, the electron-density distribution of the frontier molecular orbitals (MOs) were determined by density functional theory (DFT) using the B3LYP/LANL2DZ hybrid functional. Spatial representation of the calculated transition-involved MOs is shown in Fig. 2. Theoretical calculations reveal that, for the two dyes, the HOMO is spread over the extended π-conjugated system from the triphenylamine to the bithiophene unit, with a strong contribution of the central C≡C–Ru–C≡C fragment. It also appears that, due to the presence of the two carboxylic-acid functions, the electron density at the ground-sate is only partially located on the triphenylamine donor motif. Nonetheless, upon grafting the dyes on NiO one could expect that the withdrawing effect of the COOH groups will decrease and the electron density will subsequently slide towards the surface. On the other hand, the LUMO of the dyes is well localized on the electron-withdrawing part of the complexes, i. e. on the methylester groups in **SL1** and on the rhodanine motif in **SL2**. As a consequence, upon photoexcitation of the dye, an electron will be promoted from the metal centre towards the remote part of the molecule, thus favouring electron capture by the electrolyte. Simultaneously, electron injection to the excited dye's HOMO will be possible by hopping from NiO to the triphenylamine in contact with the metal-oxide surface.

TD-DFT calculations were further performed in order to assess the different photoinduced electronic transitions. The simulated absorption spectra are represented in Fig. S4 and the corresponding data are given in Table 2. For both dyes the simulated absorption spectrum is in good agreement with the experimental one, showing two main absorption bands, one in the visible region and one around 360 nm. In accordance with the experience, the maximum wavelength calculated for the first allowed transition, λ_{ge}, is located at 544 nm for **SL1** and strongly red-shifted for **SL2**, up to 612 nm, due to increased electron–withdrawing effect of rhodanine. Overall, the small

Table 2. Theoretical data.

Dye	ΔE_{ge} /eV [a]	λ_{ge} /nm [b]	f_{ge} [c]	Transition assignment (coefficient) [d]	Λ [e]	q_{CT} / e [f]	D_{CT} / Å [g]
SL1	2.276	544	1.842	**H→L (0.62)**; H-1→L (-0.26)	0.59	0.88	4.7
	3.359	369	0.580	H→L+1 (-0.22); H-1→L+1 (0.56); H-2→L+1 (-0.21)			
SL2	2.024	612	1.968	**H→L (0.62)**; H-1→L (0-.20)	0.58	0.90	5.1
	3.371	367	0.601	H→L+1 (0.46); H-1→L+1 (-0.39); H-2→L+1 (0.23); H-3→L+1(-0.26)			

[a] ΔE_{ge} = main transition energy. [b] λ_{ge} = calculated λ_{max}. [c] f_{ge} = oscillator strength. [d] Only the transitions with coefficients higher than 0.15 are given. [e] Λ = spatial overlap. [f] q_{CT} = quantity of transferred charge. [g] D_{CT} = distance between the barycentres of the density depletion and density increment zones related to the CT excitation.

deviation between the calculated and experimental data is attributable to the large size of such organometallic complexes.

From the calculated data (Table 2) we could further assign the origin of the main absorption bands observed on the experimental spectra. As expected, the band in the visible region owns a major HOMO→LUMO character, but also some HOMO–1→LUMO character which explains the broadness of the absorption in the visible region. As shown in Fig. 2 the electronic distribution of the HOMO-1 is fairly similar to the HOMO and both orbitals are close in energy. Consequently, the observed visible absorption band owns a full MLCT character. This is confirmed by the calculated quantity of transferred charge, q_{CT}, which is almost equal to 1. The band at higher energy also stems from multiple electronic transitions mainly from the HOMO and HOMO-1 to the LUMO+1 which is entirely located on the external phenyl rings of the triarylamine motif.

Photovoltaic measurements in p-type dye-sensitized solar cells

The photovoltaic performances of the dyes **SL1** and **SL2** were subsequently investigated in sandwich solar cells consisting of a 3 μm thick nanocrystalline layer of NiO, a platinized counter-electrode and an electrolyte based on iodide/triiodide redox couple (see experimental part for details). The metrics of the solar cells are gathered in Table 3 and the photoaction spectra are shown in Figure 3.

Table 3. Photovoltaic characteristics of the dyes **SL1** and **SL2** in p-DSC recorded under simulated solar spectrum (AM 1.5) along with dye loading on NiO film.

Dye	J_{SC} (mA/cm²)	V_{OC} (mV)	*FF* (%)	*PCE* (%)	Dye loading (nmol.cm^{-2})
SL1	2.25	104	34	0.079	31.9
SL2	1.50	77	33	0.038	10.1

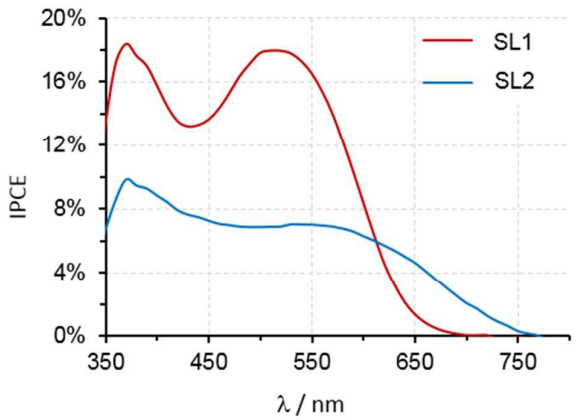

Fig. 3. Photoaction spectra of the dyes **SL1** and **SL2** in NiO based p-DSC recorded in short-circuit conditions.

The best performing dye is the red **SL1**, which produces a higher short circuit current density (J_{SC}) and a larger open circuit voltage (V_{OC}) than **SL2** (Table 3). The IPCE spectra show that **SL2** produces photocurrent above 700 nm, with a moderate efficiency, while **SL1** is more active but in a narrower bandwidth and at shorter wavelength. The IPCE (incident photon-to-current efficiency) is the factor of the light harvesting efficiency (LHE) by the injection quantum yield (ϕ_{inj}), the regeneration quantum yield (ϕ_{reg}) and the charge collection efficiency ($\phi_{collect}$) according to equation 1:

$$IPCE = LHE \times \phi_{inj} \times \phi_{reg} \times \phi_{collect} \quad (eq.1).$$

Looking at the HOMO in **SL1** and **SL2**, we can infer that the electronic coupling of the dye excited state with the NiO valence band must be quite similar as these orbitals are roughly similarly distributed over the molecule (Figure 2). Moreover, the injection driving force with **SL2** is a bit larger (albeit quite close) than that of **SL1**, indicating that the injection quantum yield is certainly not the main factor controlling the IPCE. The regeneration reaction is most certainly very high as the driving force is huge in both cases (Table 2). Desorption experiments were made and they revealed that the dye loading is 31.9 nmol/cm^2 and 10.1 nmol/cm^2 for **SL1** and **SL2**, respectively. These values are in the same range as other NiO dyes anchored with the same group N,N-di(4-benzoic acid)phenylamine (around 10-40 nmol/cm^2)[6,34-35] but much lower than the highly performing **P1** dye (123 nmol/cm^2).[36] Changing the anchoring group can certainly improve the dye loading of these complexes and consequently increase their photoconversion efficiency. In addition, the dye loading of **SL1** of three fold higher than that of **SL2**, can explain the higher J_{SC} of **SL1**, which also most certainly comes from the higher absorbance of this dye around 500 nm, where the incoming solar flux in the largest. Finally, a lower dye loading means a higher degree of naked NiO surface exposed to the electrolyte promoting more interfacial charge recombination, thus lowering the charge collection efficiency. This is evidenced by the significantly lower V_{OC} monitored for **SL2** based devices.

Conclusions

We have reported herein, the synthesis and characterization of the first ruthenium diacetylide complexes for p-DSCs. While these dyes are not perfectly optimized yet, their photovoltaic performances are relatively high if one compared with the reported ruthenium polypyridine complexes for the same application.[5-7,26] Interestingly, these two dyes display moderate injection driving force while it is accepted that the density of states of NiO valence band is lower than that of TiO_2 conduction band, that is why the sensitizers for NiO must exhibit high driving force (> 0.6 eV) to efficiently operate.[37-38] We can therefore anticipate that much better performing ruthenium diacetylide dyes can be developed by lowering the energy position of the HOMO levels to enhance injection Gibbs free enthalpy. Works are currently in progress in that direction.

Experimental section

Materials and methods

The reactions were carried out under inert atmosphere using the Schlenk techniques. Solvents were dried from appropriate drying agents (sodium for pentane, diethyl ether and THF; calcium hydride for dichloromethane, chloroform; calcium oxide for methanol) and freshly distilled under nitrogen before use. All reagents were obtained from commercially available sources and used without further purification. $[RuCl(dppe)_2][TfO]$ (**[10][TfO]**)[39] and 5'-trimethylsilylethynyl-[2,2']bithiophene-5-carbaldehyde (**5**)[40] were synthesized according to literature procedures.

^1H NMR, ^{13}C NMR and ^{31}P NMR analyses were performed on Bruker Avance III 200 MHz, Avance I 300 MHz and Avance II 400 MHz spectrometers. Chemical shift values are given in ppm with reference to solvent residual signals. HR-MS analyses were performed by the CESAMO (Bordeaux, France). Field desorption (FD) measurements were carried out on a TOF mass spectrometer AccuTOF GCv using an FD emitter with an emitter voltage of 10 kV. One to two microliters solution of the compound were deposited on a 13µm emitter wire. FT-IR spectra were recorded on a Perkin Elmer Spectrum 100 spectrometer using KBr pellets. UV-visible absorption and emission fluorescence spectra were recorded on a UV-1650PC SHIMADZU spectrophotometer and on a FluoroMax-4 HORIBA spectrofluorometer, respectively. Cyclic voltammetry analyses were performed using a potentiostat/galvanostat Autolab PGSTAT100 and a three-electrode system (working electrode: Pt disc; reference electrode: Ag/AgCl, calibrated with decamethylferrocene as internal reference; counter electrode: Pt) with 0.1M Bu_4NPF_6 as salt support at a scan rate of 200 $mV.s^{-1}$.

For the photovoltaic devices, conductive glass substrates (F-doped SnO_2) were purchased from Solaronix (TEC15, sheet resistance 15 Ω/square). The latter were successively cleaned by sonication in soapy water, then acidified ethanol for 10 min before being fired at 450 °C for 30 min. Once cooled down to room temperature, a dense layer of NiO was deposited on the FTO plates by spin coating a solution of nickel acetate (0.5 M) and triethanolamine (0.5 M) in methoxyethanol (2000 RPM, 30 s) and firing at 500°C for 30 min. Mesoporous NiO was then screen printed on the latter substrates using a home-made paste. Briefly, the NiO screen-printing paste was produced by preparing a slurry of 3 g of NiO nanopowder (Inframat) suspended in 10 mL of distilled ethanol and ball-milled (500 rpm) for 24 h. The resulting slurry was mixed in a round-bottom flask with 10 ml of 10 wt% ethanolic ethyl cellulose (Sigma Aldrich) solution and 20 ml terpineol, followed by slow ethanol removal by rotary evaporation. The dried film was calcined in air at 400 °C for 30 min. Once back at room temperature, the substrates were treated in a nickel acetate ethanolic solution (20 mM) with 1 mM triethanolamine at 60°C for 30 min and subsequently fired at 200°C for 30 min. The prepared NiO electrodes were finally soaked while still hot (80 °C) in a 0.3 mM solution of each dye during 16 h. A mixture of distilled acetonitrile and methanol was used (9/1, v/v) for each bath. Platinum counter electrodes were prepared by drop casting a few drops of an isopropanol solution of hexachloroplatinic acid in distilled isopropanol (10 mg per mL) on FTO plates (TEC7, Solaronix). Substrates were then fired at 375°C for 30 min. The photocathode and the counter electrode were placed on top of each other and sealed using a thin transparent film of Surlyn polymer (DuPont, 25 µm) as spacer. A drop of electrolyte was introduced through a predrilled hole in the counter electrode by vacuum backfilling. The electrolyte is composed of: 0.6 M 1,2-dimethyl-3-butylimidazolium iodide, 0.03 M I_2, 0.5 M 4-*tert*-butylpyridine and 0.1 M guanidinium thiocyanate in acetonitrile. The hole was then sealed by a glass stopper with Surlyn gasket. The cell had an active area of 0.25 cm^2.

The current-voltage characteristics were monitored by applying an external potential bias to the cell and measuring the photocurrent using a Keithley model 2400 digital source meter. The solar simulator is an Oriel Lamp calibrated to 100 mW/cm² , calibrated with a silicon solar cell fitted with a KG5 filter.

To avoid dye destruction in the strongly alkaline medium usually employed for desorption experiment, we developed a milder protocol: dye-sensitized substrates were placed in a glass vial containing 50 g/mL phenylphosphonic acid in dimethylformamide (2 mL). The solution immediately turns colored and after 5 to 10 min., the NiO substrate is colorless. The colored solution is then transferred to a UV-Vis cell and the absorbance at maximum wavelength is measured. The quantity of adsorbed dye is then calculated using the extinction coefficient of **SL1** and **SL2** in DMF (2.42×10^4 $M^{-1}.cm^{-1}$ at λ = 517 nm and 2.43×10^4 $M^{-1}.cm^{-1}$ at λ = 588 nm for **SL1** and **SL2** respectively) and the Beer-Lambert law.

Synthesis of 1: Methyl 4-bromobenzote (4.30 g, 20 mmol, 4 equiv.), cesium carbonate (4.89 g, 15 mmol, 3 equiv.), palladium(II) acetate (67 mg, 0.3 mmol, 6%) and aniline (0.45 mL, 5.0 mmol, 1 equiv.) were sequentially introduced in a Schlenk flask under nitrogen. Then dry toluene (50 mL) and tri-*tert*-butylphosphine (0.14 mL, 0.6 mmol, 12%) were added sequentially. The suspension was heated at 90°C for 3 days. After that, the reaction mixture was diluted with $CHCl_3$ and filtered. The resulting solution was evaporated to dryness. The crude product was purified on silica gel column (pentane/ethyl acetate (9:1, v/v)) to obtain **1** as a pale yellow powder in 63 % yield (1.14 g, 3.15 mmol). ^1H NMR (300 MHz, $CDCl_3$): δ = 7.90 (d, 4H, $^3J_{HH}$ = 9.0 Hz), 7.35 (t, 2H, $^3J_{HH}$ = 15.0 Hz), 7.22–7.14 (m, 3H), 7.08 (d, 4H, $^3J_{HH}$ = 9.0 Hz), 3.89 (s, 6H). ^{13}C NMR (75 MHz, $CDCl_3$): δ = 166.7, 151.1, 146.1, 131.1, 129.9, 126.6, 125.5, 124.2, 122.5, 52.1.

Synthesis of 2: Zinc acetate (0.25 g, 1.4 mmol, 1 equiv.) was introduced in a Schlenk tube (Schlenk tube A) under nitrogen. Dry dioxane (3 mL) and iodine monochloride (0.45 g, 2.8 mmol, 2 equiv.) were sequentially introduced in the Schlenk tube and stirred at RT for 15 min. At the same time, compound **1** (0.50 g, 1.4 mmol, 1 equiv.) was dissolved in dry dioxane (3 mL) in another Schlenk tube (Schlenk tube B). The solution of Schlenk tube B was subsequently added into Schlenk tube A with a

syringe. The solution was stirred at RT overnight. The reaction mixture was poured into saturated aqueous $Na_2S_2O_3$ solution (30 mL) to remove the excess of iodine monochloride and extracted with CH_2Cl_2. After drying on $MgSO_4$, the organic layer was evaporated to give **2** as a red-brown powder in 87 % yield (0.58 g, 1.2 mmol). ^{1}H NMR (300 MHz, $CDCl_3$): δ = 7.92 (d, 4H, $^3J_{HH}$ = 9.0 Hz), 7.63 (d, 2H, $^3J_{HH}$ = 9.0 Hz), 7.08 (d, 4H, $^3J_{HH}$ = 9.0 Hz), 6.89 (d, 2H, $^3J_{HH}$ = 9.0 Hz), 3.89 (s, 6H). ^{13}C NMR (75 MHz, $CDCl_3$): δ = 166.6, 150.6, 146.0, 138.9, 131.2, 127.9, 124.8, 123.3, 122.8, 88.9, 52.1.

Synthesis of 3: To a solution of **2** (0.48 g, 1.0 mmol, 1 equiv.), $PdCl_2(PPh_3)_2$ (35 mg, 0.05 mmol, 5%) and copper(I) iodide (5 mg, 0.025 mmol, 2.5%) in dry THF (6 mL) under nitrogen, were added Et_3N (6 mL) and (trimethylsilyl)acetylene (0.21 mL, 1.5 mmol, 1.5 equiv.). The solution was stirred at RT for 6 h. After evaporation of the solvent, the resulting crude product was purified on silica gel column (CH_2Cl_2/pentane (8:1, v/v)) to obtain **3** as a pale yellow powder in 70 % yield (0.32 g, 0.70 mmol). ^{1}H NMR (300 MHz, $CDCl_3$): δ = 7.92 (d, 4H, $^3J_{HH}$ = 9.0 Hz), 7.42 (d, 2H, $^3J_{HH}$ = 9.0 Hz), 7.08 (d, 4H, $^3J_{HH}$ = 9.0 Hz), 7.04 (d, 2H, $^3J_{HH}$ = 9.0 Hz), 3.89 (s, 6H) 0.25 (s, 18H). ^{13}C NMR (75 MHz, $CDCl_3$): δ = 166.5, 150.5, 146.2, 133.4, 131.1, 125.3, 124.7, 123.2, 123.0, 119.3, 104.4, 94.7, 52.0, -0.03.

Synthesis of 4: Compound **3** (0.68 g, 1.5 mmol, 1 equiv.) and lithium hydroxide monohydrate (0.63 g, 15.0 mmol, 10 equiv.) were introduced into a round-bottom flask under air and dissolved in a mixture of THF (8 mL) and distilled water (2 mL). The suspension was stirred at RT for 6 h. The reaction mixture was acidified with 10 % aqueous citric acid until pH 4. THF was subsequently removed through rotary evaporator and the resulting mixture was extracted with ethyl acetate. The organic layer was further washed with water, dried over $MgSO_4$ and evaporated to dryness. The crude product was obtained as a pale yellow powder in 83 % yield (0.45 g, 1.25 mmol) and used without further purification. ^{1}H NMR (300 MHz, DMSO-d6): δ = 12.81 (s, 2H), 7.89 (d, 4H, $^3J_{HH}$ = 9.0 Hz), 7.48 (d, 2H, $^3J_{HH}$ = 9.0 Hz), 7.10 (m, 6H), 3.57 (s, 1H). The intermediate compound (0.45 g, 1.25 mmol, 1 equiv.) was dissolved in dry DMF (10 mL) under nitrogen atmosphere, and HBTU (1.18 g, 3.1 mmol, 2.5 equiv.), 2-(trimethylsilyl)ethanol (0.72 mL, 5 mmol, 4 equiv.) and N,N-diisopropylethylamine (2.17 mL, 12.5 mmol, 10 equiv.) were added subsequently. The solution was stirred at RT for 48 h. After dilution with CH_2Cl_2 (20 mL), the reaction mixture was washed with saturated aqueous NH_4Cl solution and water, and then dried over $MgSO_4$ and evaporated to dryness. The crude product was purified on silica gel column (CH_2Cl_2/pentane (1:1, v/v) to CH_2Cl_2) to obtain **4** as a pale yellow powder in 65 % yield (0.45 g, 0.81 mmol). ^{1}H NMR (300 MHz, CD_2Cl_2): δ = 7.92 (d, 4H, $^3J_{HH}$ = 9.0 Hz), 7.44 (d, 2H, $^3J_{HH}$ = 9.0 Hz), 7.11 (d, 4H, $^3J_{HH}$ = 9.0 Hz), 7.08 (d, 2H, $^3J_{HH}$ = 9.0 Hz), 4.40 (m, 4H), 3.14 (s, 1H), 1.12 (m, 4H), 0.08 (s, 18H). ^{13}C NMR (75 MHz, CD_2Cl_2): δ = 166.3, 150.8, 147.2, 133.9, 131.3, 125.9, 125.6, 123.6, 118.3, 83.5, 77.6, 63.4, 17.7, -1.40.

Synthesis of 6: To a solution of 5'-trimethylsilylethynyl-[2,2']bithiophene-5-carbaldehyde (**5**) (0.25 g, 0.86 mmol, 1 equiv.) in dry $CHCl_3$ (50 ml) under nitrogen, were added piperidine (0.34 ml, 3.44 mmol, 4 equiv.) and dimethyl malonate (0.2 ml, 1.72 mmol, 2 equiv.). The solution was heated at reflux for 24 h and then evaporated to dryness. The crude product was purified on silica gel column (pentane/ethyl acetate (9:1, v/v)) to obtain **6** as an orange powder in 74 % yield (0.26 g, 0.64 mmol). ^{1}H NMR (300 MHz, CD_2Cl_2): δ = 7.80 (s, 1H), 7.29 (d, 1H, $^3J_{HH}$ = 4.0 Hz), 7.16 (d, 1H, $^3J_{HH}$ = 4.0 Hz), 7.15 (s, 1H), 7.14 (s, 1H), 3.92 (s, 3H), 3.80 (s, 3H), 0.25 (s, 9H). ^{13}C NMR (75 MHz, $CDCl_3$): δ = 166.5, 164.8, 143.2, 137.4, 136.6, 135.7, 134.9, 133.6, 124.8, 124.4, 123.7, 120.8, 101.4, 96.9, 53.0, 52.8, -0.2.

Synthesis of 7: Compound **6** (0.26 g, 0.64 mmol, 1 equiv.) was dissolved in dry THF (10 mL) under nitrogen atmosphere. Potassium carbonate (7 mg, 0.054 mmol, 0.1 equiv.) was subsequently added and the suspension was stirred at RT for 24 h. The reaction mixture was then concentrated, poured into pure water and the solution was extracted with CH_2Cl_2. After drying over $MgSO_4$, the organic layer was evaporated to dryness to afford **7** in 69 % yield (0.15 g, 0.44 mmol). ^{1}H NMR (300 MHz, $CDCl_3$): δ = 7.82 (s, 1H), 7.26 (d, 1H, $^3J_{HH}$ = 4.0 Hz), 7.17 (d, 1H, $^3J_{HH}$ = 3.9 Hz), 7.12 (d, 1H, $^3J_{HH}$ = 4.0 Hz), 7.09 (d, 1H, $^3J_{HH}$ = 3.9 Hz), 3.94 (s, 3H), 3.83 (s, 3H), 3.45 (s, 1H). ^{13}C NMR (75 MHz, THF-d8): δ = 166.4, 164.8, 143.0, 138.4, 137.3, 136.3, 135.2, 134.8, 125.7, 125.4, 123.4, 122.7, 85.1, 76.8, 52.6, 52.4.

Synthesis of 8: In a Schlenk flask under nitrogen were sequentially introduced 5'-trimethylsilylethynyl-[2,2']bithiophene-5-carbaldehyde (**5**) (0.25 g, 0.86 mmol, 1 equiv.), 3-methyl rhodanine (0.14 g, 0.95 mmol, 1.1 equiv.), ammonium acetate (0.02 g, 0.26 mmol, 0.3 equiv.) and acetic acid (5mL). The reaction mixture was left under stirring at 120°C for 3h. After cooling down to RT the reaction mixture was filtered and the solid was dissolved in CH_2Cl_2. The resulting solution was washed with pure water and then evaporated to dryness. The crude product was purified on silica gel column (CH_2Cl_2/pentane (1:1, v/v)) to obtain **8** as an orange powder in 63% yield (0.23 g, 0.54 mmol). ^{1}H NMR (300 MHz, $CDCl_3$): δ = 7.82 (s, 1H), 7.30 (d, 1H, $^3J_{HH}$ = 4.0 Hz), 7.20 (d, 1H, $^3J_{HH}$ = 4.0 Hz), 7.15 (s, 2H), 3.51 (s, 3H), 0.26 (s, 9H). ^{13}C NMR (75 MHz, $CDCl_3$): δ = 192.1, 167.4, 144.4, 137.1, 136.9, 135.2, 133.7, 125.4, 125.0, 124.1, 123.2, 120.9, 101.8, 96.8, 31.4, -0.2.

Synthesis of 9: Compound **8** (0.23 g, 0.54 mmol, 1equiv.) was dissolved in a mixture of dry THF (8 mL) and dry MeOH (2 mL) under nitrogen atmosphere. Potassium carbonate (7 mg, 0.054 mmol, 0.1 equiv.) was subsequently added and the suspension was stirred at RT for 24 h. The reaction mixture was then concentrated, poured into pure water and the solution was extracted with CH_2Cl_2. After drying over $MgSO_4$, the organic layer was evaporated to dryness to afford **9** as a dark red powder in 72 % yield (0.14 g, 0.39 mmol). ^{1}H NMR (300 MHz, DMSO-d6): δ = 8.07 (s, 1H), 7.75 (s, 1H), 7.58 (s, 1H), 7.52 (s, 1H), 7.41 (s, 1H), 4.80 (s, 1H), 3.39 (s, 3H). ^{13}C NMR (75 MHz, $CDCl_3$): δ = 192.3, 167.2, 143.8, 137.1, 135.2, 134.3, 125.7, 124.9, 124.7, 123.2, 122.5, 121.1, 83.4, 76.1, 31.2.

Synthesis of [11][TfO]: In a Schlenk tube under inert atmosphere, [RuCl(dppe)$_2$][TfO] (1) (1.08 g, 1 mmol, 1 equiv.) and **4** (0.67 g, 1.2 mmol, 1.2 equiv.) were dissolved in dry CH_2Cl_2 (50 mL). The mixture was stirred for 24 h at RT. After removal of the solvent, the crude product was washed with freshly distilled pentane (2 x 40 mL). Precipitation from a CH_2Cl_2/pentane mixture afforded pure **[10][TfO]** as a light brown powder in 93% yield (1.52 g, 0.93 mmol). ^{31}P NMR (120 MHz, $CDCl_3$): δ 35.8 (s, PPh_2). ^{1}H NMR (300 MHz, $CDCl_3$): δ 7.87 (d, 4H, $^3J_{HH}$ = 8.7 Hz), 7.34–7.07 (m, 40H), 6.88 (d, 4H, $^3J_{HH}$ = 8.7 Hz), 6.24 (d, 2H, $^3J_{HH}$ = 8.1 Hz), 5.63 (d, 2H, $^3J_{HH}$ = 8.1 Hz), 4.93 (s, 1H), 4.40 (m, 4H), 2.92 (m, 8H), 1.12 (m, 4H), 0.08 (s, 18H). ^{13}C NMR (100 MHz, CD_2Cl_2): δ 360.5, 166.6, 151.1, 144.2, 134.7, 134.5, 133.9, 133.1, 132.1, 131.9, 131.7, 131.6, 131.5, 131.2, 129.6, 129.4, 129.0, 128.8, 128.7, 126.8, 126.4, 125.5, 124.6, 124.0, 123.2, 122.8, 109.7, 63.6, 29.4, 17.9, -1.1. HR-MS FD+ (m/z): 1490.3749 ([M]$^+$, calcd. 1490.3876 for $[C_{84}H_{87}ClNO_4P_4RuSi_2]^+$). FT-IR (KBr): $\nu_{C=C}$ = 1630 cm^{-1}.

Synthesis of 12: To a solution of **[11][TfO]** (230 mg, 0.14 mmol, 1 equiv.), compound **7** (52 mg, 0.156 mmol, 1.1 equiv.) and $NaPF_6$ (47 mg, 0.28 mmol, 2 equiv.) in dry CH_2Cl_2 (15 mL) and under inert atmosphere, was added distilled Et_3N (63 µL, 0.42 mmol, 3 equiv.). The reaction mixture was stirred for 24 h at RT. The organics were further washed with degassed water and evaporated to dryness. Precipitation from a CH_2Cl_2/pentane mixture afforded pure **12** as a red solid in 89 % yield (224 mg, 0.1125 mmol). ^{31}P NMR (120 MHz, $CDCl_3$): δ = 53.4. ^{1}H NMR (300 MHz, $CDCl_3$): δ = 7.94 (d, 4H, $^3J_{H-H}$= 8.8 Hz), 7.88 (s, 1H), 7.68 (m, 8H), 7.30-6.97 (m, 39H), 6.76 (d, 2H, $^3J_{H-H}$= 8.6 Hz), 6.92 (d, 2H, $^3J_{H-H}$= 8.6 Hz), 6.10 (d, 1H, $^3J_{H-H}$= 3.8 Hz), 4.42 (m, 4H), 4.00 (s, 3H), 3.85 (s, 3H), 2.62 (m, 8H), 1.14 (m, 4H), 0.10 (s, 18H). ^{13}C NMR (100 MHz, CD_2Cl_2): δ = 166.5, 165.2, 151.3, 149.1, 146.2, 141.5, 137.7, 137.4, 136.9, 135.9, 134.7, 134.1, 132.9, 131.9, 131.4, 131.0, 129.4, 129.0, 128.6, 128.1, 127.6, 126.5, 125.8, 124.6, 122.4, 119.6, 117.6, 109.8, 63.1, 53.0, 52.8, 31.7, 30.1, 17.6, -1.3. HR-MS FD+ (m/z): 1785.4190 [M]$^+$ (calcd. 1785.4214 for $[C_{100}H_{97}NO_8P_4RuS_2Si_2]^+$). FT-IR (KBr): $\nu_{C\equiv C}$ = 2040 cm^{-1}, $\nu_{C=O}$ = 1709 cm^{-1}, $\nu_{C=C(Thiophene)}$ = 1432 cm^{-1}, ν_{C-O} = 1265 cm^{-1}, ν_{P-Ph} = 1098 cm^{-1}, ν_{Si-C} = 836 cm^{-1}.

Synthesis of SL1: To a solution of **12** (180 mg, 0.10 mmol, 1 equiv.) in dry THF (10 mL) and under inert atmosphere was added TBAF (1M sol. in THF, 0.25 mL, 0.25 mmol, 2.5 equiv.). The reaction mixture was stirred overnight at RT. After removal of the solvent the resulting solid was dissolved in CH_2Cl_2 and thoroughly washed with degassed citric acid aqueous solution (10 % m) and pure water. The organics were evaporated to dryness and the solid was further washed with pentane. Slow crystallization from a CH_2Cl_2/pentane mixture afforded pure **SL1** as a red powder in 83 % yield (132 mg, 0.083 mmol). ^{31}P NMR (120 MHz, THF-d8): δ = 53.1. ^{1}H NMR (300 MHz, THF-d8): δ = 7.86 (d, 4H, $^3J_{H-H}$= 8.7 Hz), 7.79 (s, 1H), 7.58 (m, 8H), 7.26-7.03 (m, 23H), 6.95-6.87 (m, 16H), 6.83 (d, 2H, $^3J_{H-H}$= 8.5 Hz), 6.67 (d, 2H, $^3J_{H-H}$= 8.5 Hz), 6.0 (d, 1H, $^3J_{H-H}$= 3.8 Hz), 3.90 (s, 3H), 3.75 (s, 3H), 2.53 (m, 8H). ^{13}C NMR (100 MHz, THF-d8): δ = 164.2, 162.4, 149.1, 146.2, 143.5, 139.5, 135.1, 134.9, 132.9, 132.5, 131.9, 131.3, 131.0, 129.1, 128.9, 127.3, 126.8, 126.5, 125.8, 125.1, 124.1, 123.7, 123.1, 122.7, 120.1, 119.9, 117.9, 114.4, 107.7, 49.7, 49.4, 29.3, 27.7. HR-MS FD+ (m/z): 1585.2713 [M]$^+$ (calcd. 1585.2795 for $[C_{90}H_{73}NO_8P_4RuS_2]^+$). FT-IR (KBr): $\nu_{C\equiv C}$ = 2038 cm^{-1}, $\nu_{C=O}$ = 1717-1681 cm^{-1}, $\nu_{C=C(Thiophene)}$ = 1434 cm^{-1}, ν_{C-O} = 1265 cm^{-1}, ν_{P-Ph} = 1095 cm^{-1}.

Synthesis of 13: The same procedure as for **12** was applied using **[11][TfO]** (130 mg, 0.08 mmol), **9** (33 mg, 0.095 mmol), $NaPF_6$ (27 mg, 0.16 mmol), CH_2Cl_2 (15 mL) and Et_3N (37 µL, 0.24 mmol). Pure **13** was obtained as a blue solid in 92 % yield (139 mg, 0.077 mmol). ^{31}P NMR (120 MHz, $CDCl_3$): δ = 53.2. ^{1}H NMR (300 MHz, $CDCl_3$): δ = 8.02 (d, 4H, $^3J_{H-H}$= 8.7 Hz), 7.97 (s, 1H), 7.77 (m, 8H), 7.43-7.09 (m, 42H), 7.01 (d, 2H, $^3J_{H-H}$= 8.5 Hz), 6.85 (d, 2H, $^3J_{H-H}$= 8.5 Hz), 6.19 (d, 1H, $^3J_{H-H}$= 3.8 Hz), 4.50 (m, 4H), 3.63 (s, 3H), 2.71 (m, 8H), 1.22 (m, 4H), 0.19 (s, 18H). ^{13}C NMR (150 MHz, CD_2Cl_2): δ = 192.6, 167.3, 166.1, 151.0, 150.6, 147.3, 141.1, 136.9, 136.6, 136.1, 134.6, 134.3, 133.8, 132.3, 131.5, 131.0, 130.6, 129.0, 128.9, 128.7, 127.8, 127.2, 127.1, 126.5 126.1, 125.9, 125.6, 124.3, 123.2, 122.0, 118.6, 117.5, 110.0, 62.8, 31.4, 31.2, 17.3, -1.7. HR-MS FD+ (m/z): 1800.3617 [M]$^+$ (calcd. 1800.3602 for $[C_{99}H_{94}N_2O_5P_4RuS_4Si_2]^+$). FT-IR (KBr): $\nu_{C\equiv C}$ = 2035 cm^{-1}, $\nu_{C=O}$ = 1706 cm^{-1}, $\nu_{C=C(Thiophene)}$ = 1419 cm^{-1}, ν_{C-O} = 1270 cm^{-1}, ν_{P-Ph} = 1098 cm^{-1}, ν_{Si-C} = 834 cm^{-1}.

Synthesis of SL2: Same procedure as for **SL1** was applied using **13** (100 mg, 0.056 mmol), TBAF (1M sol. in THF, 0.11 mL, 0.11 mmol) and THF (10 mL). Pure **SL2** was obtained as a blue powder in 71 % yield (63 mg, 0.039 mmol). ^{31}P NMR (120 MHz, CD_2Cl_2): δ = 53.2. ^{1}H NMR (300 MHz, CD_2Cl_2): δ = 7.81 (s, 1H), 7.80 (d, 4H, $^3J_{H-H}$= 8.5 Hz), 7.77 (m, 8H), 7.35 (d, 1H, $^3J_{H-H}$= 3.6 Hz), 7.18-6.89 (m, 38H), 6.83 (d, 2H, $^3J_{H-H}$= 8.3 Hz), 6.72 (d, 2H, $^3J_{H-H}$= 8.3 Hz), 6.09 (d, 1H, $^3J_{H-H}$= 3.6 Hz), 3.37 (s, 3H), 2.54 (m, 8H). ^{13}C NMR (150 MHz, THF-d8): δ = 192.1, 166.7, 166.1, 151.0, 150.2, 146.9, 141.4, 137.0, 136.7, 136.1, 134.7, 134.3, 133.8, 133.7, 132.8, 131.0, 130.8, 130.6, 129.0, 128.7, 128.5, 127.9, 127.7, 127.0, 126.4, 125.6, 124.8, 124.6, 123.1, 122.0, 118.8, 117.4, 110.1, 31.2, 30.4, 29.6. HR-MS FD+ (m/z): 1600.2244 [M]$^+$ (calcd. 1600.2183 for $[C_{89}H_{70}N_2O_5P_4RuS_4]^+$). FT-IR (KBr): $\nu_{C\equiv C}$ = 2034 cm^{-1}, $\nu_{C=O}$ = 1705-1686 cm^{-1}, $\nu_{C=C(Thiophene)}$ = 1420 cm^{-1}, ν_{C-O} = 1283 cm^{-1}, ν_{P-Ph} = 1097 cm^{-1}.

Acknowledgements

This work was supported by the ANR (CORuS project ANR-14-CE05-0013 and POSITIF project ANR-12-PRGE-0016-01) and the China Scholarship Council (Ph.D. grant to SL). Aurélien Planchat is acknowledged for the fabrication of the solar cells and the photovoltaic measurements (J/V characteristics and IPCE spectra). We are thankful to Mahfoudh Raissi and Nadine Szuwarski for the fabrication of NiO films on FTO substrates.

Notes and references

‡ Footnotes relating to the main text should appear here. These might include comments relevant to but not central to the matter under discussion, limited experimental and spectral data, and crystallographic data.

1 L. Duan, L. Wang, F. Li, F. Li and L. Sun, *Acc. Chem. Res.,* 2015, **48**, 2084.
2 H. Li, F. Li, B. Zhang, X. Zhou, F. Yu and L. Sun, *J. Am. Chem. Soc.*, 2015**, 137**, 4332.
3 G. C. Vougioukalakis, A. I. Philippopoulos, T. Stergiopoulos and P. Falaras, *Coord. Chem. Rev.*, 2011, **255**, 2602.
4 K. Kalyanasundaram and M. Grätzel, *Coord. Chem. Rev.*, 1998, **177**, 347.
5 C. J. Wood, K. C. D. Robson, P. I. P. Elliott, C. P. Berlinguette and E. A. Gibson, *RSC Adv.*, 2014, **4**, 5782.
6 Z. Ji, G. Natu and Y. Wu, *ACS Appl. Mater. Interfaces*, 2013, **5**, 8641.
7 Z. Ji, G. Natu, Z. Huang, O. Kokhan, X. Zhang and Y. Wu, *J. Phys. Chem.* C, 2012, **116**, 16854.
8 S. De Sousa, L. Ducasse, B. Kauffmann, T. Toupance and C. Olivier, *Chem. Eur. J.*, 2014, **20**, 7017.
9 S. De Sousa, S. Lyu, L. Ducasse, T. Toupance and C. Olivier, *J. Mater. Chem. A*, 2015, **3**, 18256.
10 F. Odobel, L. Le Pleux, Y. Pellegrin, E. Blart, *Acc. Chem. Res.*, 2010, **43**, 1063.
11 F. Odobel and Y. Pellegrin, *J. Phys. Chem. Lett.*, 2013, **4**, 2551.
12 M. Weidelener, S. Powar, H. Kast, Z. Yu, P. P. Boix, C. Li, K. Müllen, T. Geiger, S. Kuster, F. Nüesch, U. Bach, A. Mishra and P. Bäuerle, *Chem. – Asian J.*, 2014, **9**, 3251.
13 A. Nattestad, A. J. Mozer, M. K. R. Fischer, Y. B. Cheng, A. Mishra, P. Baeuerle and U. Bach, *Nat. Mater.*, 2010, **9**, 31.
14 P. Qin, H. Zhu, T. Edvinsson, G. Boschloo, A. Hagfeldt and L. Sun, *J. Am. Chem. Soc.*, 2008, **130**, 8570.
15 E. A. Gibson, A. L. Smeigh, L. Le Pleux, J. Fortage, G. Boschloo, E. Blart, Y. Pellegrin, F. Odobel, A. Hagfeldt and L. Hammarström, *Angew. Chem. Int. Ed.*, 2009, **48**, 4402.
16 A. Morandeira, J. Fortage, T. Edvinsson, L. Le Pleux, E. Blart, G. Boschloo, A. Hagfeldt, L. Hammarström and F. Odobel, *J. Phys. Chem. C*, 2008, **112**, 1721.
17 L. Le Pleux, A. L. Smeigh, E. Gibson, Y. Pellegrin, E. Blart, G. Boschloo, A. Hagfeldt, L. Hammarstrom and F. Odobel, *Energy Environ. Sci.*, 2011, **4**, 2075.
18 L. Favereau, J. Warnan, Y. Pellegrin, E. Blart, M. Boujtita, D. Jacquemin and F. Odobel, *Chem. Commun.*, 2013, **49**, 8018.
19 J. Warnan, J. Gardner, L. Le Pleux, J. Petersson, Y. Pellegrin, E. Blart, L. Hammarström and F. Odobel, *J. Phys. Chem. C*, 2013, **118**, 103.
20 C.-H. Chang, Y.-C. Chen, C.-Y. Hsu, H.-H. Chou and J. T. Lin, *Org. Lett.*, 2012, **14**, 4726.
21 C. J. Wood, G. H. Summers and E. A. Gibson, *Chem. Commun.*, 2015, **51**, 3915
22 J.-F. Lefebvre, X.-Z. Sun, J. A. Calladine, M. W. George and E. A. Gibson, *Chem. Commun.*, 2014, **50**, 5258.
23 M. Borgström, E. Blart, G. Boschloo, E. Mukhtar, A. Hagfeldt, L. Hammarström and F. Odobel, *J. Phys. Chem. B*, 2005, **109**, 22928.
24 H. Tian, J. Oscarsson, E. Gabrielsson, S. K. Eriksson, R. Lindblad, B. Xu, Y. Hao, G. Boschloo, E. M. J. Johansson, J. M. Gardner, A. Hagfeldt, H. Rensmo and L. Sun, *Sci. Rep.*, 2014, **4**, 4282.
25 A. Maufroy, L. Favereau, F. B. Anne, Y. Pellegrin, E. Blart, M. Hissler, D. Jacquemin and F. Odobel, *J. Mater. Chem. A*, 2015, **3**, 3908.
26 J. C. Freys, J. M. Gardner, L. D'Amario, A. M. Brown and L. Hammarström, *Dalton Trans.*, 2012, **41**, 13105.
27 M. Gennari, F. Légalité, L. Zhang, Y. Pellegrin, E. Blart, J. Fortage, A. M. Brown, A. Deronzier, M.-N. Collomb, M. Boujtita, D. Jacquemin, L. Hammarström and F. Odobel, *J. Phys. Chem. Lett.*, 2014, **5**, 2254.
28 F. Odobel, Y. Pellegrin, F. B. Anne and D. Jacquemin, Molecular engineering of efficient dyes for p-type semiconductor sensitization. In *High-Efficiency Solar Cells - Physics, Materials and Devices*, Wang, Z. M. W. a. X., Ed. Springer: 2013.
29 C. Olivier, B. Kim, D. Touchard and S. Rigaut, *Organometallics*, 2008, **27**, 509.
30 R. F. Winter, K. W. Klinkhammer and S. Zalis, *Organometallics*, 2001, **20**, 1317.
31 D. P. Hagberg, J. H. Yum, H. Lee, F. De Angelis, T. Marinado, K. M. Karlsson, R. Humphry-Baker, L. Sun, A. Hagfeldt, M. Grätzel and M. K. Nazeeruddin, *J. Am. Chem. Soc.*, 2008, **130** , 6259.
32 M. Weidelener, A. Mishra, A. Nattestad, S. Powar, A. J. Mozer, E. Mena-Osteritz, Y.-B. Cheng, U. Bach and P. Bauerle, *J. Mater. Chem.*, 2012, **22**, 7366.
33 G. Boschloo, E. A. Gibson and A. Hagfeldt, *J. Phys. Chem. Lett.*, 2011, **2**, 3016.
34 Z. Liu, W. Li, S. Topa, X. Xu, X. Zeng, Z. Zhao, M. Wang, W. Chen, F. Wang, Y.-B. Cheng and H. He, *ACS Appl. Mater. Interfaces*, 2014, **6**, 10614.
35 D. Ameline, S. Diring, Y. Farre, Y. Pellegrin, G. Naponiello, E. Blart, B. Charrier, D. Dini, D. Jacquemin and F. Odobel, *RSC Adv.*, 2015, **5**, 85530.
36 Y.-S. Yen, W.-T. Chen, C.-Y. Hsu, H.-H. Chou, J. T. Lin and M.-C. P. Yeh, *Org. Lett.*, 2011, **13**, 4930.
37 Z. Liu, D. Xiong, X. Xu, Q. Arooj, H. Wang, L. Yin, W. Li, H. Wu, Z. Zhao, W. Chen, M. Wang, F. Wang, Y.-B. Cheng and H. He, *ACS Appl. Mater. Interfaces*, 2014, **6**, 3448.
38 T. Daeneke, Z. Yu, G.P. Lee, D. Fu, N.W. Duffy, S. Makuta, Y. Tachibana, L. Spiccia, A. Mishra, P. Bäuerle and U. Bach, *Adv. Energy Mater.*, 2015, **5**, doi: 10.1002 / aenm.201401387.
39 J. R. Polam and L. C. Porter, *J. Coord. Chem.*, 1993, **29**, 109.
40 J.-L. Song, P. Amaladass, S.-H. Wen, K. K. Pasunooti, A. Li, Y.-L. Yu, X. Wang, W.-Q. Deng and X.-W. Liu, *New J. Chem.*, 2011, **35**, 127.

Graphical abstract

Push-pull ruthenium diacetylide complexes: new dyes for p-type dye-sensitized solar cells

Siliu Lyu, Yoann Farré, Laurent Ducasse, Yann Pellegrin, Thierry Toupance, Céline Olivier* and Fabrice Odobel*